APPLIED SCIENCES AND ENGINEERING

3D-printed automation for optimized PET radiochemistry

Alejandro Amor-Coarasa[1]*†, James M. Kelly[1†], John W. Babich[1,2,3‡]

Reproducible batch synthesis of radioligands for imaging by positron emission tomography (PET) in a manner that maximizes ligand yield, purity, and molar activity, and minimizes cost and exposure to radiation, remains a challenge, as new and synthetically complex radioligands become available. Commercially available automated synthesis units (ASUs) solve many of these challenges but are costly to install and cannot always accommodate diverse chemistries. Through a reiterative design process, we exploit the proliferation of three-dimensional (3D) printing technologies to translate optimized reaction conditions into ASUs composed of 3D-printed, electronic, and robotic parts. Our units are portable and robust and reduce radiation exposure, shorten synthesis time, and improve the yield of the final radiopharmaceutical for a fraction of the cost of a commercial ASU. These 3D-printed ASUs highlight the gains that can be made by designing a fit-for-purpose ASU to accommodate a synthesis over accommodating a synthesis to an unfit ASU.

INTRODUCTION

The diffusion and assimilation of technologies depend on their ease of use, affordability, and versatility. Three-dimensional (3D) printing now exemplifies all of these features, particularly in the breadth of its utilization, which ranges from the printing of complex biological structures (*1*) to the assembly of self-propelled microrobots (*2*). A recent compelling application of 3D printing is the creation of reaction chambers for difficult or potentially hazardous chemistries (*3*–*5*). One such chemistry could include the synthesis of radiolabeled ligands for positron emission tomography (PET). More than 2 million PET scans are performed annually in U.S. clinics alone (*6*). This number is bound to increase with the discovery of previously unidentified molecular targets, the development of next generation ligands, the availability of previously rare positron-emitting radionuclides, and the inevitable increase of the patient population. The ideal PET ligands bear radionuclides that decay within minutes to hours to limit toxicity to the patients. Therefore, the reactions that bind these radionuclides to the relevant ligands must be completed in less than one physical half-life of the radionuclide. These reactions also need to be performed with high fidelity while satisfying the regulatory concerns of administering injectable radioactive compounds to patients. Starting activities are often high to account for radioactive decay during the synthesis and transportation of the dose from the production site to the imaging suite. Consequently, radiolabeling of PET ligands for clinical imaging is now often automated by the use of commercial synthesis units that ensure a safe and effective route to specific ligands, most commonly [^{18}F]fluorodeoxyglucose ([^{18}F]FDG). As [^{18}F]FDG, which is presently the major tool for cancer diagnosis by PET, is synthesized in such bulk, commercial synthesis units are often designed with its chemistry in mind. Developments in the burgeoning field of clinical PET ligand production highlight the need for automated synthesis units (ASUs) that support emerging PET chemistries and radioligands. The combination of 3D printing and robotics can satisfy this need by producing multiple customized ASUs for a fraction of the cost of a single commercial unit. Here, we describe four ASUs assembled from 3D-printed parts and their successful production of distinct ligands bearing short-lived (half-life, $t_{1/2}$ < 2 hours) positron-emitting radionuclides for preclinical and clinical PET imaging.

RESULTS

Example 1: [^{11}C] fatty acid ASU

Kitson *et al.* (*5*) recently described the automation of chemical syntheses as an iterative process comprising a conceptual layer, a digital layer, and a physical layer. We evolved our own version of this process (Fig. 1) during the development of a [^{11}C] fatty acid ASU for radiolabeling fatty acids with carbon-11, a positron-emitting radionuclide with a decay half-life of 20 min. ^{11}C-labeled fatty acids are typically used to probe fatty acid metabolism (*7*, *8*). Substantial increases of [^{11}C]acetate uptake are observed in tumors (*9*, *10*), and deficits in [^{11}C]palmitate accumulation are noted in damaged myocardium (*11*, *12*). Our interest in PET imaging using ^{11}C-labeled short-chain fatty acids led us to develop a single cartridge for rapid [^{11}C]CO_2 trapping, labeling, and product purification (*13*). Despite improvements in yield compared to published methods, the procedure required significant user intervention, leading to excessive personnel exposure to radiation. Furthermore, reaction yields were variable because of high back pressure in the cartridge, which made it challenging to replicate the flow rate through the zeolite bed.

To address these problems and improve the synthesis of ^{11}C-labeled fatty acids, we developed a fully automated [^{11}C] fatty acid ASU. This ASU is cassette-based to simplify its use. Single-use cassettes offer numerous practical and regulatory advantages over an integrated fluidics reaction system (*14*, *15*). In addition, these cassettes and their complementary accessories, such as syringes and solid-phase extraction purification cartridges, can be purchased from a variety of commercial vendors. A full list of the cassette components for each 3D-printed ASU is provided in the Supplementary Materials.

[1]Division of Radiopharmaceutical Sciences and Molecular Imaging Innovations Institute (MI^3), Department of Radiology, Weill Cornell Medicine, New York, NY 10021, USA. [2]Sandra and Edward Meyer Cancer Center, Weill Cornell Medicine, New York, NY 10021, USA. [3]Citigroup Biomedical Imaging Center, Weill Cornell Medicine, New York, NY 10021, USA.
*Present address: Department of Radiology, Albert Einstein College of Medicine, Bronx, NY 10461, USA.
†These authors contributed equally to this work.
‡Corresponding author. Email: job2060@med.cornell.edu

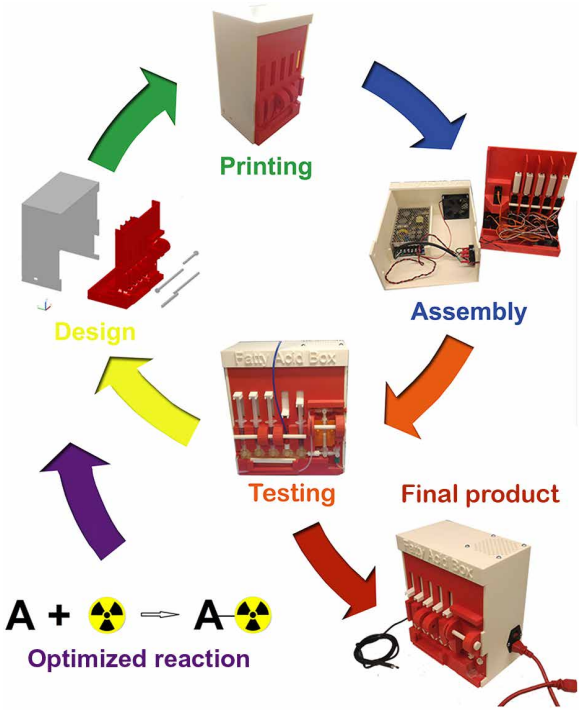

Fig. 1. The iterative process leading to radiosynthesis on a 3D-printed ASU. The optimized reaction conditions are identified ("conceptual layer") and translated into digital 3D design ("digital layer"). Digital renderings of the necessary hardware are then printed, the ASUs are assembled ("physical layer"), and the radiosynthesis is tested. At the end of the process, an optimized synthesis is translated into a fit-for-purpose ASU (photo credit: Alejandro Amor-Coarasa, Weill Cornell Medicine).

A standard five-port manifold served as the template for our design. We prepared 3D drawings of prototypes for both the moving parts and the unit housing using AutoCAD. The dimensions of the housing are 130 mm by 225 mm by 255 mm (Fig. 2), with the aim of minimizing the physical footprint of the ASU. This has the advantage of ensuring that the device can be installed in most hot cells or other shielded spaces. The AutoCAD files are available upon request.

The chemical syntheses were translated into customized sequences using the open-source Maestro software. The sequence, the second aspect of the "digital layer," defined the order of reaction steps and controlled all reaction parameters. In comparison to the software packages associated with some commercial ASUs, sequence editing in Maestro is intuitive and requires no prior experience. The digital sequence can be directly uploaded onto a microchip in the ASU. This enables the ASU to be remotely operated even without direct connection to a personal computer. The sequence encoding the radiosynthesis of ^{11}C-labeled fatty acids numbers 24 steps. The steps are described in the Supplementary Materials, and the full sequence is available upon request.

The choice of materials in which to print the ASU (the "physical layer") is determined by the function of each individual component. A broad range of materials, from simple plastic polymers to metals, is currently available for printing. Plastic polymers are more economical but are often less resistant to mechanical force and contact with organic solvents than metallic materials. However, 3D-printed metals are also significantly heavier than the plastics. In concert with a small physical footprint, we also aimed to minimize the mass of the ASU without compromising its performance. By printing the housing in acrylonitrile butadiene styrene (ABS), we are able to restrict the weight of the ASU to 4 kg. By comparison, commercial ASUs can weigh up to 40 kg. ABS is not resistant to organic solvent, but our cassette-based design confines organic materials to the sterile plastic manifold. We chose to print actuators, syringe drivers, and other pieces of support in nylon as this material is more robust than ABS. Some of the moving parts of the ASU are subjected to significant mechanical forces. When printed in nylon, the syringe drivers are strong enough to overcome the pressure that builds up during addition of the Grignard reagent to the zeolite-containing cartridge. During prototype development, the force exerted by the syringe drivers was sufficient to displace the cassette. Therefore, a reinforcing nylon brace was added to the cassette, and no mechanical failures were observed in more than 20 subsequent syntheses.

Benchtop robotic devices now perform multiple chemical reactions and explore new chemical spaces (*16*). The integration of inexpensive miniature robotic parts into a 3D-printed structure creates exciting opportunities for reaction automation and increases the scope of reactions that can be undertaken. Robotic parts perform important functions during the synthesis, such as transfer of reagents and solvents from the cassette to the zeolite cartridge, with precision and fidelity. These devices allow us to overcome the limitations of the manual synthesis and deliver higher yields of ^{11}C-labeled fatty acids while simultaneously decreasing synthesis time. A full list of parts is provided in the Supplementary Materials.

The performance of the [^{11}C] fatty acid ASU was evaluated for the production of [^{11}C]acetate, [^{11}C]palmitate, and [^{11}C]propionate, which may be used as a precursor for enzymatic synthesis of succinate (*17*) or as a synthon for more complex molecules (*18*, *19*). Each synthesis comprises four components: [^{11}C]CO_2 trapping, addition of the Grignard precursor, purification of the crude product, and elution of the final compound (Fig. 2). The [^{11}C] fatty acid ASU produces [^{11}C]acetate (n = 5) and [^{11}C]palmitate (n = 12) with 62.8 ± 8.3% and 57.2 ± 12.4% decay-corrected radiochemical yields (dcRCYs), respectively, corrected to the start of synthesis (Table 1). The yield of [^{11}C]propionate (n = 3) is 24.4 ± 5.1% due to the formation of multiple by-products resulting from over-alkylation. [^{11}C]Acetate and [^{11}C]propionate are purified from radiochemical impurities by solid-phase extraction. Each of the acids is isolated in greater than 97% radiochemical purity (RCP), and synthesis time is less than 6.5 min from [^{11}C]CO_2 delivery.

By comparison, our manual synthesis of [^{11}C]palmitate using the 13X molecular sieve cartridge is completed in 8 min and results in a dcRCY of 38 ± 7% (*13*). Despite the short synthesis, our custom-built ASU achieves a nearly 20% reduction in overall synthesis time. End-of-synthesis yield, as well as dcRCY, is substantially higher. The synthesis of [^{11}C]acetate on commercial ASUs is reported to be 40 to 55% dcRCY, with a total synthesis time ranging from 8 to 20 min (*20*–*22*). Similarly, automated syntheses of [^{11}C]palmitate afford 33 to 40% dcRCY with 9 to 36 min of total synthesis time (*21*–*23*). In contrast to our single-cartridge approach, these syntheses typically bubble [^{11}C]CO_2 through a solution of Grignard reagent in diethyl ether. This approach may necessitate physical modifications to be made to the ASU (*22*) that must be removed before the ASU can be returned to routine production of other radiotracers. Even when solutions can be found to avoid physical modifications, synthesis time is longer and dcRCY is lower than can be achieved with the 3D-printed [^{11}C] fatty acid ASU.

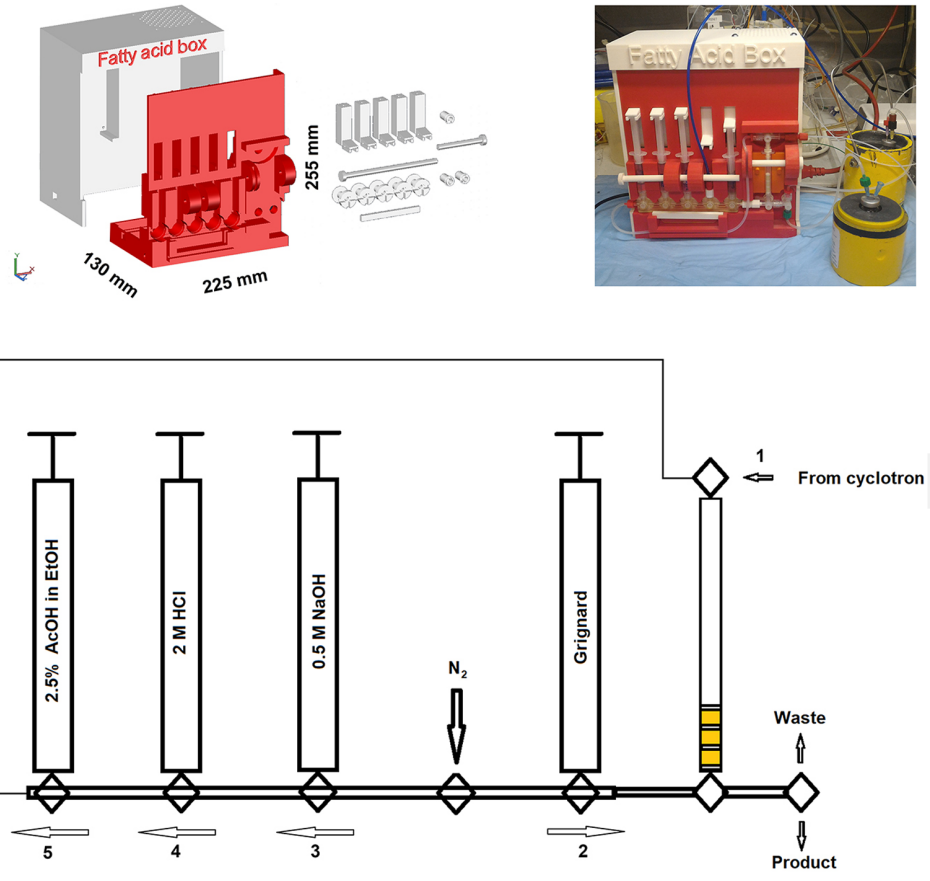

Fig. 2. The [^{11}C] fatty acid ASU design and dimensions. The ASU is assembled as a single module incorporating a cassette consisting of a five-port manifold, four syringes, and a polypropylene cartridge containing three stages of either zeolite 13X or Dowex 1X8. The syringe drivers are printed in nylon, and the housing is printed in ABS. The synthesis consists of five steps, beginning with [^{11}C]CO_2 trapping and ending with elution of the final product (photo credit: Alejandro Amor-Coarasa, Weill Cornell Medicine).

Example 2: [^{18}F] dual heater ASU

PET imaging of metastatic castrate-resistant prostate cancer using small molecules that target prostate-specific membrane antigen (PSMA) is currently under clinical evaluation at numerous centers across the world (*24*). Tracers such as [^{68}Ga]PSMA-11 are sensitive and specific (*25*). However, the physical limitations of ^{68}Ga currently render it unsuitable to cater to the volume of patients with prostate cancer expected to require routine scanning. Fluorine-18 is better suited to meet expected clinical demands. [^{18}F]DCFPyL (2-(3-{1-carboxy-5-[(6-[18F]fluoro-pyridine-3-carbonyl)-amino]-pentyl}-ureido)-pentanedioic acid) and [^{18}F]PSMA-1007 successfully delineate tumors in patients with prostate cancer, albeit with certain limitations (*26*, *27*), and [^{18}F]RPS-040 is a promising alternative with an improved tissue distribution in preclinical models (*28*).

The multistep radiosynthesis of [^{18}F]RPS-040 for preclinical PET imaging was first performed manually and involved two separate reactions and a distillation. Two reactors are used to maximize the chemical purity and RCP of the crude triazole product, thereby increasing reaction yield and simplifying the purification procedure (*28*). Although the use of two reactors improved the yield of [^{18}F]RPS-040, their use presented multiple challenges to the automation of the radiosynthesis. Relatively few commercially available ASUs contain two reactors. [^{18}F]FEA could conceivably be collected into an external vessel and then returned to the reactor for the click reaction, but this modification would almost certainly decrease the amount of available azide. This is because trapping of [^{18}F]FEA is enhanced at lower temperatures. We therefore designed and assembled the [^{18}F] dual heater ASU (Fig. 3) to perform the first automated synthesis of [^{18}F]RPS-040. The syringe drivers are printed in nylon and the housing is printed in ABS, but in this case, we elected to use glass reactors. Glass is more resistant to temperature and solvent than even the most robust plastics, such as polypropylene, and offers the additional advantage of being easily cleaned. This allowed us to reuse the reactors during the optimization process to reduce the costs of method development. To maximize the rate of thermal conductivity between the heating element and the reactor, we 3D-printed the reactor heating jacket in porcelain.

These choices of materials for our "physical layer" translate to significant improvements in reaction time. The use of a Peltier element and a constant flow of compressed air directed at the base of the

Table 1. Summary of key parameters for the syntheses performed with the 3D-printed ASUs. Radiochemical yield (RCY) is decay-corrected to the start of synthesis and is expressed as yield ± SD. Radiochemical purity (RCP) was determined by radio HPLC and is expressed as purity ± SD. Synthesis time is defined as the time interval between the button push to initiate the sequence and the isolation of the final radiopharmaceutical in a sterile vial.

ASU	Radiotracer	dcRCY (%)	RCP (%)	*n*	Time
Fatty acid	[^{11}C]Acetate	62.8 ± 8.3	97.5 ± 1.0	5	5.3 min
Fatty acid	[^{11}C]Propionate	24.4 ± 5.1	99.7 ± 0.2	3	5.3 min
Fatty acid	[^{11}C]Palmitate	57.2 ± 12.4	96.7 ± 0.8	12	6.5 min
Dual heater	[^{18}F]RPS-040	15.2 ± 3.6	>95	9	65 min
Multidrug	[^{68}Ga]PSMA-11	90.7 ± 0.5	>99.9	3	15 min
Multidrug	[^{68}Ga]DOTATOC	89.0 ± 0.3	>99.9	3	15 min
Millifluidic	[^{68}Ga]PSMA-11	89.4 ± 3.7	>99.9	3	5 min
Millifluidic	[^{68}Ga]DOTATOC	49.4 ± 9.3	98.5 ± 1.3	3	5 min

heater cool the second reactor (Fig. 3) to less than 5°C even when the temperature in the adjacent reactor exceeds 130°C. A thermostat controls the temperature in each heater. The cooled reactor warms from 5° to 100°C in only 2 min to perform the click reaction. The rapid changes in reaction temperature play a significant role in reducing the time of synthesis from 100 min, as in our manual method (*28*), to 65 min. No mechanical failures were observed in any of the 15 testing and validation runs.

The reaction comprises seven steps (Fig. 3), and its corresponding sequence incorporates 63 individual processing steps. A summary of the sequence is available in the Supplementary Materials. By contrast, automated sequences for even simple syntheses, such as the synthesis of [^{18}F]FDG, on most commercially available ASUs exceed 200 steps. This difference highlights the simplified translation of chemical process to digital processes that can be achieved using a built-for-purpose 3D-printed ASU.

Initiation of the sequence is controlled by a remote control button that is affixed magnetically to the exterior face of the hot cell. Three checkpoints are programmed. The synthesis pauses at each checkpoint until a push of the button triggers the next step in the sequence. The synthesis of [^{18}F]RPS-040 (n = 9) is accomplished with 15.2 ± 3.6% dcRCY in 65 min from [^{18}F]fluoride trapping (Table 1). Residual activity in the first reactor is less than 10% of the starting activity, suggesting that [^{18}F]fluoride incorporation into [^{18}F]FEA is high, and the distillation is efficient. No significant escape of radioactivity is observed during the distillation. Only trace amounts of residual activity remain in the second reactor after transfer of the contents for high-performance liquid chromatography (HPLC) purification. The purified product is isolated in greater than 95% RCP. In comparison to the manual synthesis, the yield of the click reaction is slightly reduced, perhaps due to a higher volume of MeCN in the reaction. Nevertheless, the yield of [^{18}F]RPS-040 by the automated approach is comparable to its yield by manual synthesis. We are currently optimizing solvent proportions and reaction volumes to further improve our promising early results.

Example 3: [^{68}Ga] multidrug ASU

The clinical importance of ^{68}Ga-labeled peptide radiopharmaceuticals continues to grow, especially in the field of oncology (*29*). One factor driving the growth of ^{68}Ga PET is the increased availability of the radionuclide. Typically, ^{68}Ga is produced by elution of a ^{68}Ge/^{68}Ga generator, and direct use of the eluate for radiolabeling saves valuable time, as the half-life of ^{68}Ga is 68 min, as well as reduces radiation exposure. Automated synthesis modules are available on the market, but many require adaptations for routine clinical use (*30*). We have successfully used the iQS ^{68}Ga Fluidic Labeling Module supplied by iTG for the production of [^{68}Ga]PSMA-11 and [^{68}Ga]DOTATOC [(DOTA^0-Phe^1-Tyr^3)octreotide] for ongoing clinical studies at our facility (*31*). However, this manual system requires multiple operations that introduce the possibility of user error.

We designed the [^{68}Ga] multidrug ASU to create a fully automated benchtop unit for routine production of ^{68}Ga-labeled radiopharmaceuticals in a radiopharmacy (Fig. 4). Some of the features of the "physical layer" of the [^{18}F] dual heater ASU are retained, including the glass reactor, the nylon syringe drivers, and the 3D-printed housing in ABS. New features were introduced to accommodate the specific requirements of the metalation reaction. As reaction temperatures are not required to exceed 95°C, the reactor casing is also printed in ABS. The thermocouple is inserted into the casing to enable temperature control. Heat from the heating element was conducted to the reactor by means of a copper coil. The reactor could be heated from room temperature to 90°C in approximately 1 min and maintained at 90°C without any warping or deformation of the materials. We used a syringe pump, printed in ABS, to regulate elution of the generator. We also retained a cassette-based design to enhance microbiological safety. The cassette is based on the iQS fluidics and incorporates filters to ensure that all liquids and gases that come into contact with the final product maintain sterility.

The design integrated generator elution, precursor labeling, and product purification and formulation. The synthesis is initiated by pressing a button built into the top face of the ASU (Fig. 4). The generator eluate is collected in the reactor (Fig. 4, step 2) and incubated with a premixed solution of precursor ligand in buffer. Purification of the reaction mixture is performed by solid-phase extraction (Fig. 4, step 3). Last, the product is eluted and formulated in 8.3% v/v EtOH in normal saline (Fig. 4, step 4) and released for quality control testing. The sequence encoding the synthesis numbers 57 steps, and the duration of the sequence is 15 min.

The total synthesis time is comparable to our manual synthesis using the Fluidic Labeling Module. Both [^{68}Ga]PSMA-11 (n = 3) and [^{68}Ga]DOTATOC (n = 3) are isolated with approximately 90% dcRCY (corrected to start of synthesis) and greater than 99% RCP (Table 1). Each product is sterile and pyrogen free and complies with all criteria for batch release. The yields of [^{68}Ga]PSMA-11 and

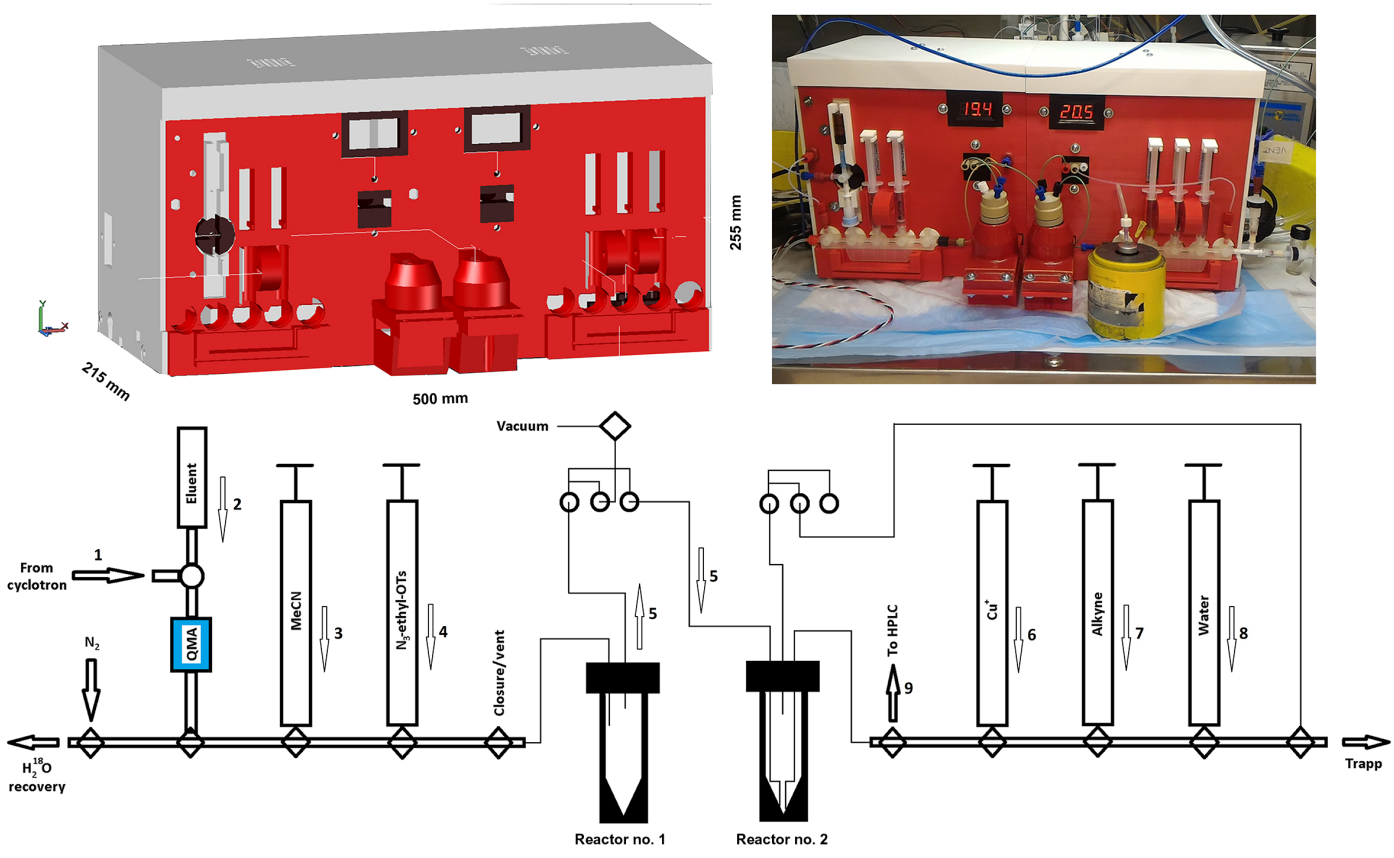

Fig. 3. The [^{18}F] dual heater ASU design and dimensions. The cassette-based ASU is a single module incorporating two glass reactors. Temperature control is achieved by a thermostat. The temperature of the first reactor ranges from 25° to 150°C, and the temperature of the second reactor ranges from <5° to 150°C. The reactor casing is printed in porcelain, the syringe drivers are printed in nylon, and the housing is printed in ABS. The synthesis constitutes nine steps. The first four steps, resulting in synthesis of 2-[^{18}F]fluoroethylazide, take place in the first reactor. Following transfer of this synthon to the second reactor by distillation, [^{18}F]RPS-040 is produced by a click reaction and transferred for HPLC purification (photo credit: Alejandro Amor-Coarasa, Weill Cornell Medicine).

[^{68}Ga]DOTATOC represent a slight improvement on yields previously reported for the synthesis of these tracers using the iQS ^{68}Ga Fluidic Labeling Module and the same ^{68}Ge/^{68}Ga generator (*31*). Despite the high back pressure of the generator, the 3D-printed syringe pump successfully operated at a constant flow, and no failures (either mechanical or in the synthesis) occurred throughout the development process. Thus, the [^{68}Ga] multidrug ASU performs at least as well as manual synthesis and significantly reduces the risks associated with manual user operations.

Example 4: [^{68}Ga] millifluidic ASU

Although the yields of [^{68}Ga]PSMA-11 and [^{68}Ga]DOTATOC on the [^{68}Ga] multidrug ASU are excellent, the incubation of the reaction materials in the reactor is relatively lengthy. As the maximum activity of ^{68}Ga eluted from the ^{68}Ge/^{68}Ga generator is currently limited to <3.7 GBq, any improvement in the end-of-synthesis activity of the ^{68}Ga-labeled radiopharmaceutical translates to an additional patient dose, approximately 100 to 150 MBq. We sought to reduce synthesis time by using a continuous flow reaction approach. This approach eliminates the incubation step. Continuous flow processes have been used to reduce reaction times and reagent amounts in a variety of organic and bio-organic reactions (*32*). Recently, microfluidic continuous flow approaches have also been applied to radiochemical synthesis (*33*, *34*).

The design of a continuous flow reactor for radiochemistry must weigh the advantages of a microfluidics system with the drawbacks of using tubing with a very narrow diameter. The back pressure from the generator is significant, and direct elution into a microfluidics system carries an increased risk of mechanical stress and obstructions forming in the tubing. The relatively high salt content of the buffer also increases the possibility of material precipitating within the reactor coil. Blockages due to solid material in the tubing are one of the major causes of nonuniform flow and inefficient mixing in continuous flow systems (*32*). Therefore, we designed the [^{68}Ga] millifluidic ASU (Fig. 5) for the proof-of-concept millifluidic radiolabeling of small molecules with ^{68}Ga. The reaction coil is fashioned from stainless steel HPLC tubing with an outer diameter of $^{1}/_{16}$ inch and housed in a 3D-printed porcelain heater for maximum thermal conductivity. A dual syringe pump, printed in ABS, simultaneously regulates the elution of the generator and the addition of the premixed precursor/buffering solution. The remaining features are identical to the [^{68}Ga] multidrug ASU.

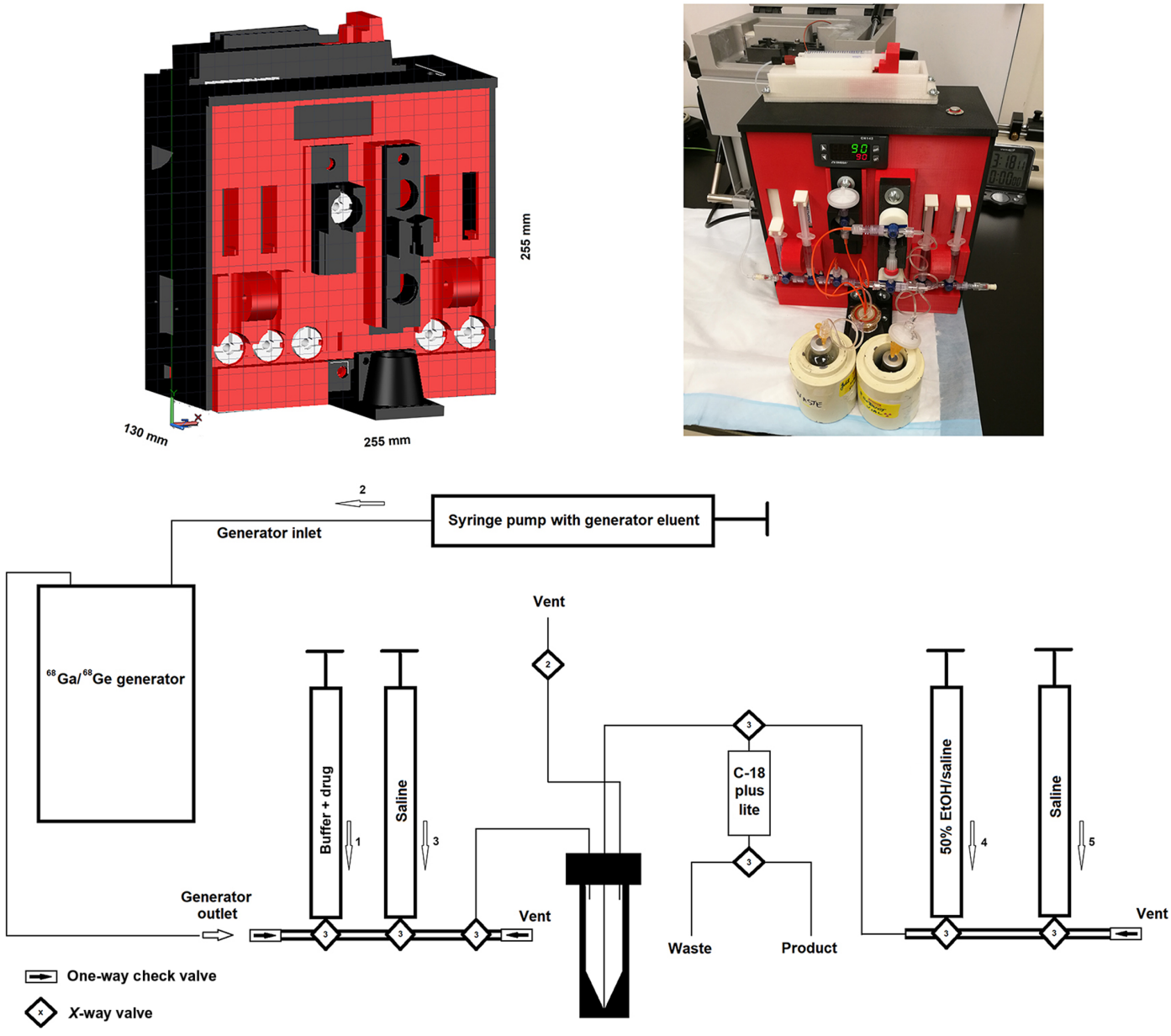

Fig. 4. The [^{68}Ga] multidrug ASU design and dimensions. The unit is a single module with an integrated 3D-printed syringe pump. The polycarbonate cassette is adapted from the iQS fluidic module. The housing and reactor casing are printed in ABS. The synthesis is conceived as five processes. Using the syringe pump, the ^{68}Ge/^{68}Ga generator is directly eluted into the reactor, which contains the precursor ligand and buffer. After incubation for 5 min at 90°C, the labeled products are purified by solid-phase extraction and collected in a vial after sterile filtration (photo credit: Alejandro Amor-Coarasa, Weill Cornell Medicine).

The synthesis consists of mixing the generator eluate and the buffered precursor solution in a t-valve (Fig. 5, step 1), passing the mixture through the heated reaction coil, and purification of the labeled products by solid-phase extraction (Fig. 5, step 2). The flow rate of precursor addition is matched to the elution of the generator to produce a homogeneous flow and to ensure appropriate reaction stoichiometry. The labeled product is eluted from the purification cartridge and reformulated in 8.3% v/v EtOH in saline in a sterile vial. A total of 25 steps are included in the sequence. Through efficient temperature changes, including the heating of the reactor coil from room temperature to 90°C in approximately 20 s, and the continuous flow, the total reaction time is only 5 min. By contrast, the synthesis using the [^{68}Ga] multidrug ASU lasts almost 15 min.

The yield and RCP of [^{68}Ga]PSMA-11 (n = 3) are unchanged relative to the [^{68}Ga] multidrug ASU production, but the yield of [^{68}Ga]DOTATOC (n = 3) decreased to 49.4 ± 9.3%, decay-corrected to the start of synthesis (Table 1). In this latter synthesis, the remaining activity is collected in the waste vial, consistent with it being free

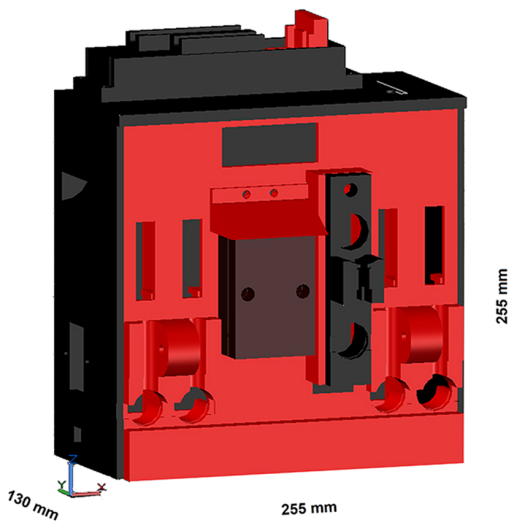

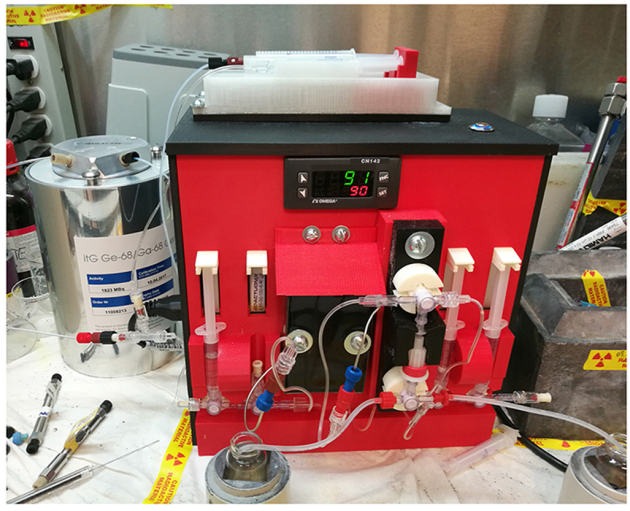

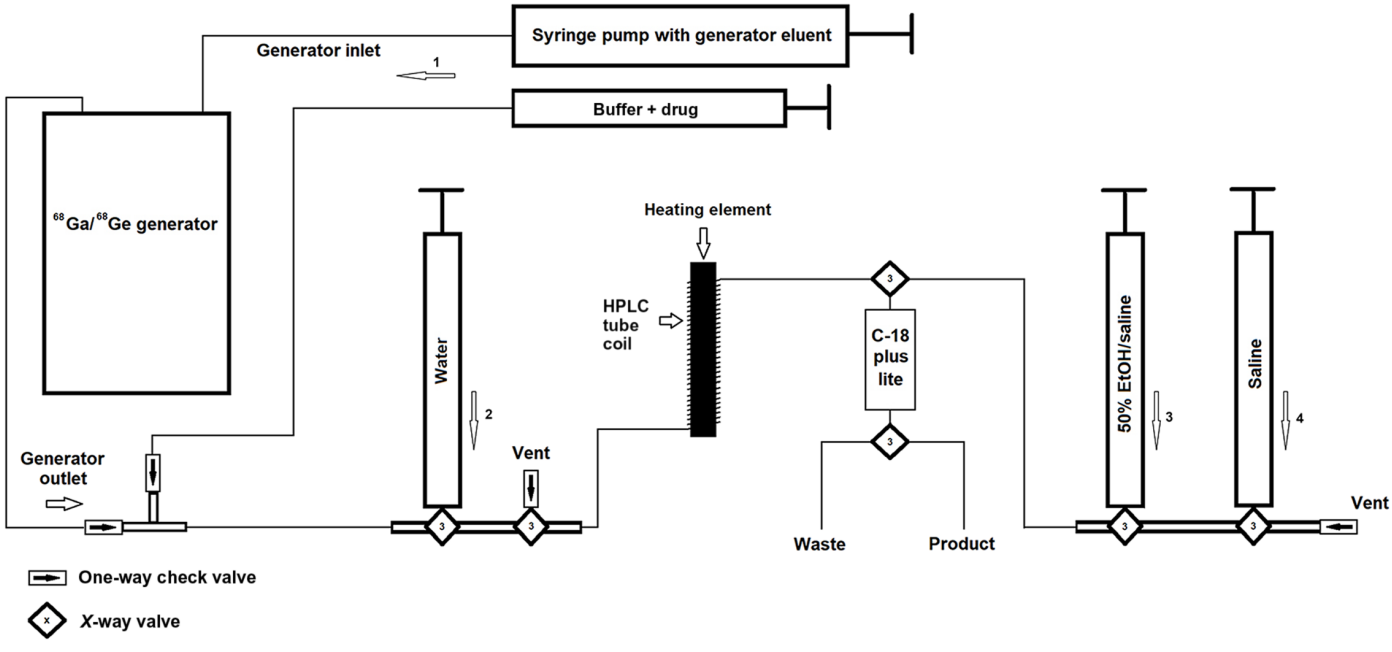

Fig. 5. The [^{68}Ga] millifluidic ASU design and dimensions. The unit consists of a single module with an integrated syringe pump and reaction coil. The polycarbonate cassette is adapted from the iQS fluidics system. The generator is eluted in a continuous flow and mixes with the precursor solution before reaching the reaction coil. Approximately 1 m of $^{1}/_{16}$-inch HPLC stainless steel tubing is coiled around the heating element and enclosed in 3D-printed porcelain. The syringe drivers are printed in nylon, and the housing is printed in ABS. The product is purified by solid-phase extraction and eluted to a sterile vial (photo credit: Alejandro Amor-Coarasa, Weill Cornell Medicine).

$^{68}Ga^{3+}$. The low labeling yield is attributed to the slower kinetics of ^{68}Ga chelation by DOTA relative to the HBED-CC chelator. Nevertheless, the yield of [^{68}Ga]DOTATOC is comparable to the yield achieved by microfluidic synthesis (*35*), but the larger tube diameters improve the reliability of the synthesis by eliminating obstructions in the tubing and reactor. We expect that a slower flow through the reaction coil, which can be achieved by modifying the motor on the syringe pump, would improve labeling yield. Further optimization of flow rates and reaction conditions may be possible, but our proof-of-concept studies using the [^{68}Ga] millifluidic ASU support the currently underexplored millifluidic continuous flow approach to radiosynthesis.

DISCUSSION

Routine production and distribution of radiopharmaceuticals requires large starting activities (>37 GBq) and presents considerable challenges with respect to product fidelity and personnel safety. Consequently, automated radiosynthesis has become a central feature of radiopharmaceutical

production (*36*). Early automation developed over time into streamlined, self-contained, commercially available modular ASUs. The ASUs generally fall into two categories—cassette-based systems and stationary systems with permanent fluidics—and typically share a retail price of well over US$100,000. In addition, these ASUs often occupy a large physical footprint, leading to further investment in laboratory space and infrastructure for radiation protection.

Despite a recent trend toward increasing the amount and complexity of the hardware incorporated in ASUs, the design of most of these devices is optimized for two to three organic reactions followed by a single cartridge- or HPLC-based purification (*37*). Implementation of more complex, multistep syntheses on these ASUs is challenging and sometimes impossible. When new chemistries require automation, the prohibitively high price of ASUs renders the purchase of a new unit economically unjustifiable for tracer development and preclinical evaluation.

To overcome these obstacles to radioligand development, we propose a philosophical shift in synthesis automation: Rather than compromising reaction yield or purity by implementing the synthesis on an unfit ASU, design a fit-for-purpose ASU on which to optimize the synthesis. The proliferation of 3D printing technologies makes this possible and economically attractive. We demonstrate with the development of 3D-printed ASUs that a broad scope of radiolabeling reactions can be translated into digital sequences. In turn, devices assembled from common, inexpensive electronic, robotic, and custom-designed 3D-printed parts performed the sequence with high fidelity. The four ASUs were constructed for a total cost of parts that varied from US$1200 for the [^{11}C] fatty acid ASU to US$7000 for the [^{18}F] dual heater ASU. This cost includes all materials associated with the design, prototyping, and final printing and assembly, but not the labor costs. Subsequent identical ASUs can be produced for approximately 60% of the cost of the first units due to elimination of the prototyping phase. The flexibility of the technology allows the devices to be modified according to the requirements of each laboratory or local regulatory agency. For example, new components, such as pin diode radiation detectors, can be integrated with minimal hardware wiring. The housing of the ASU could be printed in even more robust materials, such as stainless steel, with only an incremental increase in the cost of assembly. Last, each piece of hardware can be easily and inexpensively replaced in the event of failure. Although we have not observed a single failure in more than 40 syntheses to date, electric motors are thought to be susceptible to radiation. However, as the retail price of each motor is less than US$20, multiple backups can be maintained in stock. If production volume requires at least one ASU to be operational at all times, then entire redundant ASUs can be assembled. We estimate that 20 3D-printed ASUs could be prepared for the same cost as a single commercial ASU. The reduced costs democratize the technology and allow laboratories of different sizes and in different environments to conceive, digitize, and automate the synthesis of many different radiopharmaceuticals.

The reduced physical footprint of the 3D-printed ASUs contributes further to their value. In contrast to 3D-printed devices used for chemical synthesis, which reduce operator intervention and exposure to potentially hazardous substances, 3D ASUs for radiochemistry must also be designed to reduce exposure to radiation. In part, this requires their size to be small enough to be shielded in a hot cell or behind lead shielding on a benchtop. It also requires the radiosynthesis to be operated remotely or by a simple button push, to enable the operator to be positioned at a safe distance during the synthesis. We use a simple push button to initiate the reaction sequence and demonstrate that the button can be located directly on the ASU or on a remote control placed outside the hot cell. Last, the light weight of the ASUs enables carry in–carry out radiosynthesis. The portability of our 3D-printed ASU is a major attribute because it permits multiple units to be used even when few hot cells are available. Alternatively, it allows a backup unit to be substituted for an ASU requiring maintenance without halting production. By swapping the ASUs in and out of a fixed synthesis space, laboratories can greatly increase the number of radiotracers that can be synthesized without having to make major infrastructural changes.

The potential for 3D-printed ASUs to satisfy unmet needs in radiopharmaceutical development and production continues to grow. Each of the four units reduced synthesis time relative to existing methods, thereby gaining both increased final activity and molar activity of the product. These gains may ultimately support a higher volume of patient imaging. In addition, the emerging field of targeted alpha therapy represents an exciting application for 3D-printed ASUs. Initial clinical evaluation of DOTATOC (*38*) and PSMA-617 (*39*), labeled with ^{225}Ac, hints at promising antitumor effects. The bifunctional isothiocyanate derivative of macropa-NCS chelator rapidly and quantitatively complexes [^{225}Ac]Ac^{3+} when conjugated to small molecules (*40*). The mild conditions for chelation, including precursor concentrations in the low micromolar range and a 1 M NH_4OAc buffer at pH 5 to 6, are suitable for continuous flow radiolabeling. Radiosynthesis of ^{225}Ac-labeled molecules on a 3D-printed millifluidic ASU dedicated to this purpose may prove highly valuable as the demand for these radioligands increases. It would also prove valuable in the unlikely event of contamination with the long-lived ^{225}Ac ($t_{1/2}$ = 10 days). The contaminated ASU could be removed and stored for decay without affecting the synthesis of other radiopharmaceuticals at the facility. Digitization of the synthesis and automation of the process will secure a steady supply of the radioligand, standardize the method under the appropriate regulatory framework, and reduce operator exposure to radiation.

MATERIALS AND METHODS

3D printing of parts and housing

The designs of the 3D-printed ASUs can be found in Figs. 2 to 5. Designs for the ASU housing were drawn using AutoCAD (Autodesk, USA) and printed in ABS on a Fortus 250mc 3D printer (Stratasys, USA). Printing was performed at the Clinical and Translational Science Center (CTSC) 3-D Printing Core Facility (Weill Cornell Medicine, New York, USA).

Parts were drawn using AutoCAD (Autodesk, USA). All parts printed in ABS, such as reactor housing and syringe pumps, were printed on a Fortus 250mc 3D printer (Stratasys, USA) at the CTSC 3-D Printing Core Facility (Weill Cornell Medicine, New York, USA). Materials printed in nylon, such as syringe drivers and valves, or in porcelain, such as reactor housing, were printed by Shapeways (New York, USA). AutoCAD drawings are available upon request.

Robotic and electronic parts

A full list of parts can be found in the Supplementary Materials (table S1). Parts were purchased from commercial vendors (table S2) and assembled in-house.

Cassette design and assembly

Schematic representation of the cassettes can be found in Figs. 2 to 5. High-resolution photographs of the fully assembled ASUs and cassettes are presented in figs. S1 to S4. Videos of the syntheses performed by the [^{11}C] fatty acid ASU and the [^{18}F] dual heater ASU are available in the electronic Supplementary Materials. The cassettes for the [^{11}C] fatty acid ASU and the [^{18}F] dual heater ASU were based on a five-port, dimethyl sulfoxide (DMSO)–resistant manifold (ABX, Germany), while the cassettes for the [^{68}Ga] multidrug ASU and the [^{68}Ga] millifluidic ASU were based on the polycarbonate iQS Fluidic Labeling Module (ABX, Germany). The cassettes incorporated plastic syringes, cartridges for solid-phase extraction, and reactors, as depicted in Figs. 2 to 5. A full list of parts and suppliers is provided in the Supplementary Materials (tables S3 and S4). With the exception of glass reactors, which were washed with water and acetone, and dried overnight at 90°C, all other components of the cassette were treated as single-use parts and were discarded at the end of the synthesis.

Radiosynthesis

[^{11}C] Fatty acid ASU

All chemicals and reagents were purchased from Sigma-Aldrich (St. Louis, USA) and used without further purification unless otherwise specified. Compressed N_2 gas and compressed air were supplied by Tech Air (USA). Molecular sieve 13X, 100 to 120 mesh, (Supelco) was stored in a vacuum desiccator and otherwise used without further preparation. Dowex 1X8-200 was washed with diethyl ether and stored in a vacuum desiccator. The cartridge was prepared as previously described (*13*). One frit was removed from an Extract Clean 1.5-ml Filter (Grace Davison Discovery Sciences). A stage of 100 mg (±1.5 mg) of resin (either zeolite 13X or Dowex 1X8) was packed in the cartridge and compressed with the plunger of a 1-ml disposable syringe. The stage was capped with a 20-μm polyethylene frit for a 1.5-ml reservoir (Grace Davison Discovery Sciences). Two more stages of 100 mg (±1.5 mg) of resin were prepared and capped in the manner described. A polypropylene cartridge adapter (Agilent) and a polypropylene one-way valve (VWR) were added to the top of the column. A three-way valve (VWR) was fitted to the bottom of the column. The packed column was stored in a vacuum desiccator for at least 2 hours before use. RCP was assessed by radio HPLC using an Eckert & Ziegler Flow-Count Radio-HPLC Detector and a Varian Dynamax HPLC. Radiochemical yield was defined as the ratio of final purified product activity to initial radioisotope activity and corrected for decay to start of synthesis.

[^{11}C]Acetate

No-carrier-added [^{11}C]CO_2 was generated by a [^{14}N(p,α)^{11}C] reaction in a TR-19 Cyclotron (Advanced Cyclotron Systems, Inc.). It was transferred to the ASU in a steady flow of N_2 and trapped on the 13X zeolite column. The column consisted of two stages of Dowex 1X8 (the bottom stages) and one stage of molecular sieve 13X. The exhaust gas flowed through the waste vial and was filtered before release in an ascarite column to trap any remaining radioactive gas. Following trapping, the zeolite-containing cartridge was sealed at the top, and 0.7 ml of a 1 M solution of methylmagnesium bromide in dibutyl ether was introduced through the bottom valve. After addition of the reagent, the pressurized cartridge was isolated by sealing the bottom vial. Following a 5-min reaction at room temperature, the pressure was released by venting to the waste vial. The column was then dried by a 30-s flow of N_2 before it was eluted with 3 ml of H_2O. The product was filtered through a preactivated Sep-Pak C18 Plus cartridge (Waters, USA) and a 0.22-μm sterile filter (Millex) into a sterile vial.

RCP was determined on a PRP-X100 anion exchange column (Hamilton, USA) using an isocratic 0.4 M KH_2PO_4 + 0.5% v/v MeCN mobile phase at a flow rate of 1 ml/min. The retention time of [^{11}C]acetate was 3.7 ± 0.1 min.

[^{11}C]Propionate

The synthesis was performed as described above, using 0.7 ml of a 3 M solution of ethylmagnesium bromide in diethyl ether. The retention time of [^{11}C]propionate was 5.1 ± 0.2 min.

[^{11}C]Palmitate

The [^{11}C]CO_2 production and trapping were performed as described above. The zeolite column consisted of 3 × 100-mg stages of molecular sieve 13X. After the top of the column was sealed, 0.7 ml of a 0.5 M solution of pentadecylmagnesium bromide in diethyl ether was added through the bottom valve. The bottom valve was closed, and the reaction was allowed to proceed for 5 min at room temperature. Next, the pressure was released by venting to the waste vial. The zeolite column was washed through the top valve with 1 ml of 0.5 M NaOH and dried by a 30-s flow of N_2. A second wash with 3 ml of 2 M HCl was performed, followed by 30 s of drying. Last, the column was eluted to a filtered, sterile vial with 1 ml of a 2.5% v/v AcOH/EtOH solution.

RCP was determined by analytical HPLC using a Waters Symmetry C18 (5 μm, 4.6 × 50 mm) analytical column. The method was a gradient from 0 to 100% B at a flow rate of 2 ml/min, according to the following schedule: 0 to 2 min, 0% B; 2 to 5 min, 0 to 100% B; 5 to 10 min, 100% B; 10 to 12 min, 100 to 0% B. Mobile phase A consisted of H_2O + 0.1% trifluoroacetic acid (TFA). Phase B consisted of a 90/10 v/v solution of MeCN/H_2O + 0.1% TFA. The retention time of [^{11}C]palmitic acid was 7.6 ± 0.2 min.

[^{18}F] Dual heater ASU

All solvents and reagents were purchased from Sigma-Aldrich (St. Louis, USA) and were of reagent-grade quality unless otherwise indicated. Analytical and semi-prep HPLC was performed on a dual-pump Varian HPLC (Agilent Technologies) fitted with a dual ultraviolet-visible light detector and an NaI(Tl) detector (BioScan). Mobile phase A was H_2O + 0.01% TFA, and phase B was 90:10 v/v MeCN:H_2O + 0.1% TFA. Semiprep HPLC was performed on a μBondapak C18 7.8 × 300-mm, 125-Å column (Waters), while analytical HPLC was performed on a Symmetry C18 4.6 × 50-mm, 100-Å column (Waters). The ultraviolet absorption spectrum was monitored at 220 and 280 nm. Semiprep HPLC was performed using an isocratic solvent mixture of 15% B at a flow rate of 4 ml/min. Analytical HPLC was performed at a flow rate of 2 ml/min using the following gradient: 0 to 1 min, 0% B; 1 to 8 min, 0 to 100% B; 8 to 10 min: 100 to 0% B.

[^{18}F]RPS-040

No-carrier-added ^{18}F was generated by a ^{18}O(p,n)^{18}F reaction in a TR19 Cyclotron (Advanced Cyclotron Systems, Inc.) and trapped on a quarternary methyl ammonium (QMA) cartridge (Waters). The cartridge was dried with N_2 and the water was recovered. The QMA was eluted with 1 ml of an 80% v/v MeCN/H_2O solution containing 5 mg of K_2CO_3 and 10 mg of K_{222} by opening the system to the first reactor and evacuating the cassette. The elution vial was sequentially pressurized with two cycles of N_2 addition and evacuated by pulling from the evacuated reaction vial to maximize the volume of eluent transferred. The $^{18}F^-$ was dried in the reactor at 100°C for 15 min,

including three sequential 5-min azeotropic drying steps using 0.5 ml of MeCN.

Once the drying procedure was completed, the temperature in the reactor was reduced to 80°C, and 0.5 ml of a solution (20 mg/ml) of 2-azidoethyltosylate in 80% v/v DMSO/MeCN was added to the reactor. The reaction proceeded for 10 min at 80°C, at which point the temperature was allowed to slowly increase to 130°C for an additional 10 min. The temperature of the second reactor was simultaneously cooled to <5°C. As the first reactor warmed, a flow of N_2 from this reactor to the second reactor was initiated. This facilitated the distillation of [^{18}F]fluoroethylazide. The second reactor contained 100 μl of *N*,*N*′-dimethylformamide (DMF) and was maintained at 2° to 6°C during the collection period. To purge the transfer lines, the N_2 flow persisted as the first reactor was cooled from 130°C to room temperature over 2 min using compressed air.

Then, the premixed Cu^+ solution, consisting of 50 μl of 0.5 M $CuSO_4$ and 50 μl of 1.5 M sodium ascorbate in 100 μl of DMF, and the alkyne precursor, a solution of 2 mg in 100 μl of DMF, were added to the second reactor. The temperature of the second reactor was ramped to 100°C for 15 min. It was then cooled to room temperature using compressed air, and the contents of the reactor were transferred to an external vial through the indicated position on the cassette (Fig. 3). The reactor was washed three times with 1 ml of H_2O, and the washes were combined in the external vial, resulting in a final volume of 4 ml. The crude product was purified by semiprep HPLC as previously described (*28*) and reformulated in an isotonic 10% v/v EtOH/saline solution.

[^{68}Ga] Multidrug ASU

$^{68}Ga^{3+}$ was supplied by a ^{68}Ge/^{68}Ga itG generator (12 to 18 months old from time of calibration; ITM, Germany) that had been retired from clinical production. The typical elution activity at start of synthesis was 370 to 740 MBq. HCl and NaOAc were purchased from Sigma-Aldrich (USA) and were traceSELECT (>99.999%) for trace analysis quality. The precursors for PSMA-11 and DOTATOC were purchased from ABX (Germany). Ethanol was 200 proof and was purchased from VWR (USA). The iQS ^{68}Ga Fluidic Labeling Module was purchased from ITM (Germany) and used with the small modifications noted below.

[^{68}Ga]PSMA-11

The reactor was heated to 90°C over the course of approximately 1 min. Then, the premixed solution of 5 μg of PSMA-11 in buffer (1 ml of 0.24 M NaOAc) was added to the reactor. Following addition of the precursor, the generator was eluted with 4 ml of 0.05 M HCl. Elution was completed after 3 min, and the eluate was directly transferred to the reaction vial. The reaction mixture was incubated for 5 min. Upon completion of the reaction, the buffer syringe was filled with air filtered through a 0.2-μm filter. The air was used to pressurize the reactor, initiating the flow of the reaction mixture from the reactor to the C18 cartridge. This procedure was repeated four times to maximize volume transfer. The material that was not retained on the cartridge was collected in the waste vial. Then, 3 ml of saline was added to the reactor. The same syringe was used to pressurize the reactor and transfer the saline through the C18 cartridge as described above. Following the saline wash, the C18 cartridge valve was opened to the filtered sterile product vial. The cartridge was eluted with 0.6 ml of a 50% ethanol solution, followed by 3 ml of sterile saline. To maximize product recovery, air was loaded into the sterile saline syringe pushed through the C18 cartridge. The process was repeated an additional three times. The product was subjected to full batch release quality control assessment, including appearance, pH, chemical purity and RCP, filter integrity, endotoxin content, and sterility, as previously described (*31*).

[^{68}Ga]DOTATOC

The synthesis was performed as described above, using 25 μg of DOTATOC.

[^{68}Ga] Millifluidic ASU

$^{68}Ga^{3+}$ was supplied by a ^{68}Ge/^{68}Ga itG generator (12 to 18 months old from time of calibration; ITM, Germany) that had been retired from clinical production. The typical elution activity at start of synthesis was 370 to 740 MBq. HCl and NaOAc were purchased from Sigma-Aldrich (USA) and were traceSELECT (>99.999%) for trace analysis quality. The precursors for PSMA-11 and DOTATOC were purchased from ABX (Germany). Ethanol was 200 proof and was purchased from VWR (USA). The iQS ^{68}Ga Fluidic Labeling Module was purchased from ITM (Germany) and used with the small modifications noted below.

[^{68}Ga]PSMA-11

The reactor coil was heated to 90°C in approximately 20 s. Then the buffer, containing 5 μg of PSMA-11 in 1.5 ml of a 0.16 M NaOAc solution, and 4 ml of 0.05 M HCl eluent were pushed simultaneously with the same syringe pump to ensure equal speed of addition. The eluent passed through the generator before mixing with the precursor-containing buffer in the T link. The mixture continuously flowed through the T link, the reactor, and the C18 cartridge. The material that was not retained on the C18 cartridge was collected in a waste vial. After elution was completed, H_2O was pushed through the reactor coil and the C18 cartridge and collected in the waste. Filtered air (3 ml) was drawn into the water syringe and passed through the reactor coil to maximize volume transfer. The procedure was repeated a further three times. Last, the C18 cartridge was eluted with 0.6 ml of a 50% ethanol solution, followed by 3 ml of sterile saline. To maximize product recovery, air was loaded into the sterile saline syringe pushed through the C18 cartridge. The process was repeated an additional three times.

[^{68}Ga]DOTATOC

The synthesis was performed as described above, using 25 μg of DOTATOC. At end of the synthesis, the waste vial was collected and analyzed by radio HPLC to determine the identity of the radioactive species.

Reaction sequences

Sequences were programmed using Maestro open-source software. The steps for each sequence are reported in the Supplementary Materials. Full details, including step duration and/or parameter set point, are available upon request.

SUPPLEMENTARY MATERIALS

Supplementary material for this article is available at http://advances.sciencemag.org/cgi/content/full/5/9/eaax4762/DC1

Fig. S1. Photograph of the fully assembled [^{11}C] fatty acid ASU.
Fig. S2. Photograph of the fully assembled [^{18}F] dual heater ASU.
Fig. S3. Photograph of the fully assembled [^{68}Ga] multidrug ASU.
Fig. S4. Photograph of the fully assembled [^{68}Ga] millifluidic ASU.
Table S1. Parts list for each of the 3D-printed ASUs.
Table S2. Suppliers of robotic and electronic parts.
Table S3. Cassette components and parts used for each ASU.
Table S4. Suppliers of cassette parts.
Movie S1. Fatty acid ASU.
Movie S2. Dual heater ASU.
Section S1. Reaction sequences

REFERENCES AND NOTES

1. D. B. Kolesky, K. A. Homan, M. A. Skylar-Scott, J. A. Lewis, Three-dimensional bioprinting of thick vascularized tissues. *Proc. Natl. Acad. Sci. U.S.A.* **113**, 3179–3184 (2016).
2. Z. Yan, M. Han, Y. Shi, A. Badea, Y. Yang, A. Kulkarni, E. Hanson, M. E. Kandel, X. Wen, F. Zhang, Y. Luo, Q. Lin, H. Zhang, X. Guo, Y. Huang, K. Nan, S. Jia, A. W. Oraham, M. B. Mevis, J. Lim, X. Guo, M. Gao, W. Ryu, K. J. Yu, B. G. Nicolau, A. Petronico, S. S. Rubakhin, J. Lou, P. M. Ajayan, K. Thornton, G. Popescu, D. Fang, J. V. Sweedler, P. V. Braun, H. Zhang, R. G. Nuzzo, Y. Huang, Y. Zhang, J. A. Rogers, Three-dimensional mesostructures as high-temperature growth templates, electronic cellular scaffolds, and self-propelled microbots. *Proc. Natl. Acad. Sci. U.S.A.* **114**, E9455–E9464 (2017).
3. V. Dragone, V. Sans, M. H. Rosnes, P. J. Kitson, L. Cronin, 3D-printed devices for continuous-flow organic chemistry. *Beilstein J. Org. Chem.* **9**, 951–959 (2013).
4. P. J. Kitson, S. Glatzel, W. Chen, C.-G. Lin, Y.-F. Song, L. Cronin, 3D printing of versatile reactionware for chemical synthesis. *Nat. Protoc.* **11**, 920–936 (2016).
5. P. J. Kitson, G. Marie, J.-P. Francoia, S. S. Zalesskiy, R. C. Sigerson, J. S. Mathieson, L. Cronin, Digitization of multistep organic synthesis in reactionware for on-demand pharmaceuticals. *Science* **359**, 314–319 (2018).
6. J. Czernin, M. Allen-Auerbach, D. Nathanson, K. Herrmann, PET/CT in oncology: Current status and perspectives. *Curr. Radiol. Rep.* **1**, 177–190 (2013).
7. N. Tamaki, K. Morita, Y. Kuge, E. Tsukamoto, The role of fatty acids in cardiac imaging. *J. Nucl. Med.* **41**, 1525–1534 (2000).
8. I. Grassi, C. Nanni, V. Allegri, J. J. Morigi, G. C. Montini, P. Castellucci, S. Fanti, The clinical use of PET with ^{11}C-acetate. *Am. J. Nucl. Med. Mol. Imaging* **2**, 33–47 (2012).
9. N. Oyama, H. Akino, H. Kanamaru, Y. Suzuki, S. Muramoto, Y. Yonekura, N. Sadato, K. Yamamoto, K. Okada, ^{11}C-acetate PET imaging of prostate cancer. *J. Nucl. Med.* **43**, 181–186 (2002).
10. C.-L. Ho, S. C. H. Yu, D. W. C. Yeung, ^{11}C-acetate PET imaging in hepatocellular carcinoma and other liver masses. *J. Nucl. Med.* **44**, 213–221 (2003).
11. E. M. Geltman, Assessment of myocardial fatty acid metabolism with 1-^{11}C-palmitate. *J. Nucl. Cardiol.* **1**, S15–S22 (1994).
12. H. Miyabe, N. Ohte, A. Iida, H. Narita, T. Yoshida, G. Kimura, Evaluation of fatty acid β-oxidation in patients with prior myocardial infarction in relation to myocardial blood flow, total oxidative metabolism, and left ventricular wall motion. *Circ. J.* **69**, 1459–1465 (2005).
13. A. Amor-Coarasa, J. M. Kelly, J. W. Babich, Synthesis of [^{11}C]palmitic acid for PET imaging using a single molecular sieve 13X cartridge for reagent trapping, radiolabeling and selective purification. *Nucl. Med. Biol.* **42**, 685–690 (2015).
14. J. Collins, C. M. Waldmann, C. Drake, R. Slavik, N. S. Ha, M. Sergeev, M. Lazari, B. Shen, F. T. Chin, M. Moore, S. Sadeghi, M. E. Phelps, J. M. Murphy, R. M. van Dam, Production of diverse PET probes with limited resources: 24 ^{18}F-labeled compounds with a single radiosynthesizer. *Proc. Natl. Acad. Sci. U.S.A.* **114**, 11309–11314 (2017).
15. S. Thompson, M. R. Kilbourn, P. J. H. Scott, Radiochemistry, PET imaging, and the internet of chemical things. *ACS Cent. Sci.* **2**, 497–505 (2016).
16. J. M. Granda, L. Donina, V. Dragone, D.-L. Long, L. Cronin, Controlling an organic synthesis robot with machine learning to search for new reactivity. *Nature* **559**, 377–381 (2018).
17. T. L. Collier, Y. Hwang, R. Ramasamy, R. R. Sciacca, K. T. Hickey, N. R. Simpson, S. R. Bergmann, Synthesis and initial evaluation of 17-^{11}C-heptadecanoic acid for measurement of myocardial fatty acid metabolism. *J. Nucl. Med.* **43**, 1707–1714 (2002).
18. R. J. Davenport, V. W. Pike, K. Dowsett, D. R. Turton, K. Poole, Automated chemoenzymatic synthesis of no-carrier-added [*carbonyl*-^{11}C]propionyl L-carnitine for pharmacokinetic studies. *Appl. Radiat. Isot.* **48**, 917–924 (1997).
19. C. Rami-Mark, J. Ungersboeck, D. Haeusler, L. Nics, C. Philippe, M. Mitterhauser, M. Willeit, R. Lanzenberger, G. Karanikas, W. Wadsak, Reliable set-up for in-loop ^{11}C-carboxylations using Grignard reactions for the preparation of [*carbonyl*-^{11}C]WAY-100635 and [^{11}C]-(+)-PHNO. *Appl. Radiat. Isot.* **82**, 75–80 (2013).
20. X. Tang, G. Tang, D. Nie, Fully automated synthesis of ^{11}C-acetate as tumor PET tracer by simple modified solid-phase extraction purification. *Appl. Radiat. Isot.* **82**, 81–86 (2013).
21. B. H. Mock, C. Brown-Proctor, M. A. Green, B. Steele, B. E. Glick-Wilson, Q.-H. Zheng, An automated SPE-based high-yield radiosynthesis of [^{11}C]acetate and [^{11}C]palmitate: No liquid-liquid extraction, solvent evaporation or distillation required. *Nucl. Med. Biol.* **38**, 1135–1142 (2011).
22. A. C. Runkle, X. Shao, L. J. M. Tluczek, B. D. Henderson, B. G. Hockley, P. J. H. Scott, Automated production of [^{11}C]acetate and [^{11}C]palmitate using a modified GE Tracerlab $FX_{C\text{-}Pro}$. *Appl. Radiat. Isot.* **69**, 691–698 (2011).
23. P. Fang, M. Jacobson, R. Schwandt, J. Christensen, R. Bruhnke, S. Corner, C. Koutsari, G. Wiseman, M. Jensen, Fully automated synthesis module for [C-11] palmitic acid. *J. Nucl. Med.* **51**, 2082 (2010).
24. M. S. Hofman, R. J. Hicks, T. Maurer, M. Eiber, Prostate-specific membrane antigen: Clinical utility in prostate cancer, normal patterns, pearls, and pitfalls. *Radiographics* **38**, 200–217 (2018).
25. M. Perera, N. Papa, D. Christidis, D. Wetherell, M. S. Hofman, D. G. Murphy, D. Bolton, N. Lawrentschuk, Sensitivity, specificity, and predictors of positive ^{68}Ga-prostate-specific membrane antigen positron emission tomography in advanced prostate cancer: A systematic review and meta-analysis. *Eur. Urol.* **70**, 926–937 (2016).
26. F. L. Giesel, L. Will, I. Lawal, T. Lengana, C. Kratochwil, M. Vorster, O. Neels, F. Reyneke, U. Haberkorn, K. Kopka, M. Sathekge, Intraindividual comparison of ^{18}F-PSMA-1007 and ^{18}F-DCFPyL PET/CT in the prospective evaluation of patients with newly diagnosed prostate carcinoma: A pilot study. *J. Nucl. Med.* **59**, 1076–1080 (2018).
27. F. L. Giesel, B. Hadaschik, J. Cardinale, J. Radtke, M. Vinsensia, W. Lehnert, C. Kesch, Y. Tolstov, S. Singer, N. Grabe, S. Duensing, M. Schäfer, O. C. Neels, W. Mier, U. Haberkorn, K. Kopka, C. Kratochwil, F-18 labelled PSMA-1007: Biodistribution, radiation dosimetry and histopathological validation of tumor lesions in prostate cancer patients. *Eur. J. Nucl. Med. Mol. Imaging* **44**, 678–688 (2017).
28. J. Kelly, A. Amor-Coarasa, A. Nikolopoulou, D. Kim, C. Williams Jr., S. Ponnala, J. W. Babich, Synthesis and pre-clinical evaluation of a new class of high-affinity ^{18}F-labeled PSMA ligands for detection of prostate cancer by PET imaging. *Eur. J. Nucl. Med. Mol. Imaging* **44**, 647–661 (2017).
29. I. Velikyan, ^{68}Ga-based radiopharmaceuticals: Production and application relationship. *Molecules* **20**, 12913–12943 (2015).
30. L. Uccelli, A. Boschi, C. Cittanti, P. Martini, L. Lodi, E. Zappaterra, S. Romani, S. Zaccaria, D. Cecconi, I. Rambaldi, I. Santi, S. Panareo, M. Giganti, M. Bartolomei, Automated synthesis of ^{68}Ga-DOTA-TOC with a cationic purification system: Evaluation of methodological and technical aspects in routine preparations. *Curr. Radiopharm.* **11**, 130–137 (2018).
31. A. Amor-Coarasa, M. Schoendorf, M. Meckel, S. Vallabhajosula, J. W. Babich, Comprehensive quality control of the ITG ^{68}Ge/^{68}Ga generator and synthesis of ^{68}Ga-DOTATOC and ^{68}Ga-PSMA-HBED-CC for clinical imaging. *J. Nucl. Med.* **57**, 1402–1405 (2016).
32. F. M. Akwi, P. Watts, Continuous flow chemistry: Where are we now? Recent applications, challenges and limitations. *Chem. Commun.* **54**, 13894–13928 (2018).
33. Z. Liu, K. S. Schaap, L. Ballemans, R. de Zanger, E. de Blois, M. Rohde, E. Oehlke, Measurement of reaction kinetics of [^{177}Lu]Lu-DOTA-TATE using a microfluidic system. *Dalton Trans.* **46**, 14669–14676 (2017).
34. S. Pfaff, C. Philippe, V. Pichler, M. Hacker, M. Mitterhauser, W. Wadsak, Microfluidic ^{68}Ga-labeling: A proof of principle study. *Dalton Trans.* **47**, 5997–6004 (2018).
35. A. Amor-Coarasa, J. M. Kelly, J. W. Babich, Microfluidics assisted labeling of ^{68}Ga-DOTATOC. Advantages and limitations. *Eur. J. Nucl. Med. Mol. Imaging* **42**, S199 (2015).
36. G. B. Saha, Synthesis of PET radiopharmaceuticals, in *Basics of PET Imaging: Physics, Chemistry, and Regulations* (Springer-Verlag, 2005), pp. 111–124.
37. S. Li, A. Schmitz, H. Lee, R. H. Mach, Automation of the radiosynthesis of six different ^{18}F-labeled radiotracers on the AllinOne. *EJNMMI Radiopharm. Chem.* **1**, 15 (2017).
38. C. Kratochwil, F. Bruchertseifer, F. Giesel, C. Apostolidis, U. Haberkorn, A. Morgenstern, Ac-225-DOTATOC—An empiric dose finding for alpha particle emitter based radionuclide therapy of neuroendocrine tumors. *J. Nucl. Med.* **56**, 1232 (2015).
39. C. Kratochwil, F. Bruchertseifer, F. L. Giesel, M. Weis, F. A. Verburg, F. Mottaghy, K. Kopka, C. Apostolidis, U. Haberkorn, A. Morgenstern, ^{225}Ac-PSMA-617 for PSMA-targeted α-radiation therapy of metastatic castration-resistant prostate cancer. *J. Nucl. Med.* **57**, 1941–1944 (2016).
40. N. A. Thiele, V. Brown, J. M. Kelly, A. Amor-Coarasa, U. Jermilova, S. N. MacMillan, A. Nikolopoulou, S. Ponnala, C. F. Ramogida, A. K. H. Robertson, C. Rodríguez-Rodríguez, P. Schaffer, C. Williams Jr., J. W. Babich, V. Radchenko, J. J. Wilson, An eighteen-membered macrocyclic ligand for actinium-225 targeted alpha therapy. *Angew. Chem. Int. Ed.* **56**, 14712–14717 (2017).

Acknowledgments: We acknowledge T. M. Jeitner for helpful contributions to manuscript preparation. **Funding:** This work was funded in part by the Clinical and Translational Science Center at Weill Cornell Medicine through a Cooperative Agreement awarded by the National Center for Advancing Translational Sciences (grant no. 5 UL1 TR000457-07). **Author contributions:** A.A.-C., J.M.K., and J.W.B. designed the research. A.A.-C. and J.M.K. performed the research and acquired the data. A.A.-C. analyzed the data. J.M.K. wrote the manuscript. A.A.-C. and J.W.B. edited the manuscript. **Competing interests:** The authors declare that they have no competing interests. **Data and materials availability:** All data needed to evaluate the conclusions in the paper are present in the paper and/or the Supplementary Materials. Additional data related to this paper may be requested from the authors.

Submitted 26 March 2019
Accepted 13 August 2019
Published 13 September 2019
10.1126/sciadv.aax4762

Citation: A. Amor-Coarasa, J. M. Kelly, J. W. Babich, 3D-printed automation for optimized PET radiochemistry. *Sci. Adv.* **5**, eaax4762 (2019).